SLAC-TN-71-5
T. M. Jenkins
March 1971

# SHIELDING OF PHOTONS FOR SPEAR

## I. Introduction

Most of the shielding done at SLAC is based on the early works of DeStaebler.[1] In the years since DeStaebler did his calculations, many reports have appeared in the literature, and measurements have been made which modify some of the early results somewhat. For example, a new value for the neutron removal mean free path in earth of 116 g/cm$^2$ was published by a joint LRL-CERN-RHEL[2] effort which modified the early SLAC value of 158 g/cm$^2$.

In shielding SPEAR, an approach should be taken which is different than that used to shield the two-mile long accelerator. The SPEAR machine is circular, and also normally operates with a stored beam. That is, there are a finite number of electrons to shield against when the stored beam is considered.

Partly because of this situation, and partly because the beam may be scraping at shallow angles with a subsequent high intensity of photons, neutrons may not be the dominating form of radiation which must be shielded against. This is because only a small fraction ($\sim$ 1%) of the energy goes into the production of all nuclear particles when the beam is fully attenuated. In the case of glancing angles, the shower may not fully develop, and consequently the photon to neutron ratio may be greatly increased. Furthermore, if the absolute number of neutrons is decreased, then the shield thickness for neutron shielding alone will decrease, and in very thin shields around an electron accelerator, photons may dominate.

Shielding of photons produced by high energy electron beams has not been treated comprehensively in the literature. The photon energy emerging from a target is not unambiguous, especially from targets that are not entirely absorbing. The angular intensity distribution of ionizing radiation was treated in TN-70-34[3] for the cases of a 2 GeV electron beam obliquely incident upon a collimator, and upon thick and thin flat plates. The energy distribution was not covered.

The purpose of this note is to discuss the techniques of photon shielding, and to provide recipes for shielding which should be applicable to machines such as SPEAR.

II. Beam Stopped in a Thick Target

In SPEAR, lead collimators are located at various points[4] around the machine (at the exit ends of magnets, for example) to intercept errant beams. Glasstone[5] and Price et al.,[6] give a simple rule to use in the shielding of photons, using a composite shield where a heavy material (high Z) is followed by a light material (low Z). The rule is: whenever the initial photon energy is high (above the minimum in the mass absorption coefficient for the heavier material), the photons entering the lighter material may be assumed to have the energy associated with the attenuation minimum in the heavier material, and the buildup factor in the light material is determined for that energy.

Some attempts may be made to test the validity of the rule. From the results of shower measurements,[7] the longitudinal fall-off in energy deposition has a slope similar to the slope of photons having an energy associated with the minimum in the attenuation coefficient. This would tend to substantiate the rule.

It is possible to test it more carefully, however. Nagel,[8] in a Monte Carlo analysis of showers in lead, shows a relative photon energy distribution at a depth of seven shower-maxima, shown in Fig. 1. This distribution is independent of incoming electron energy, at least above 100 MeV. The average energy of this distribution may be shown to be very close to 3 MeV which is the energy of photons at the attenuation minimum for lead. Using 3 MeV, and the buildup factor associated with 3 MeV photons in concrete, the upper curve of Fig. 2 (curve A) is constructed. The transmission without buildup is shown as curve C.

There may be some error in using an average energy for the photons, and the buildup factor associated with that average energy. To test this, the spectrum of Fig. 1 was divided into smaller energy intervals, and the buildup factor for each energy interval applied to the fraction of the photons in that interval. The transmission of each interval was then summed, and the resultant curve (curve B) drawn in Fig. 2. The agreement with the average photon energy transmission curve is quite good.

Perhaps it would be justifiable to review briefly what is meant by attenuation coefficients and buildup factors. While there have been many publications on this topic, this report will draw mainly upon a forthcoming book by K. Kase and W. R. Nelson[9] which provides an excellent summary. They note five coefficients in use, the first three of which are given official sanction by the ICRU. These

coefficients are:

1. Mass attenuation coefficient, $(\mu/\rho)$.
2. Mass energy transfer coefficient $(\mu_K/\rho)$.
3. Mass energy absorption coefficient $(\mu_{en}/\rho)$.

4 and 5. Both called mass absorption coefficients, and are modifications of no. 2.

The first, mass attenuation coefficient, $(\mu/\rho)$, is often referred to as the 'narrow beam' cross section, and is given by

$$(\mu/\rho) = \frac{1}{\rho}(\tau + \sigma + \sigma_R + K) \tag{1}$$

where $\tau$ = photoelectric cross section

$\sigma$ = Compton (or incoherent scatter) cross section

$\sigma_R$ = Raleigh (or coherent scatter) cross section

K = Pair production cross section

$\rho$ = Density

The other four coefficients are similar, and may be treated together for purposes of this report. Briefly, the mass energy transfer coefficient, $(\mu_K/\rho)$ allows for the escape of fluorescent radiation, the fraction of energy carried off in the Compton process by the electron, and the annihilation of a positron with an atomic electron, and is given by

$$(\mu_K/\rho) = \frac{1}{\rho}\left[\tau(1-f) + \sigma\frac{\bar{E}}{h\nu} + K\left(1 - \frac{2mc^2}{h\nu}\right)\right] \tag{2}$$

If the fraction, G, of energy which escapes in the form of bremsstrahlung is accounted for, then we get the mass energy absorption coefficient, $(\mu_{en}/\rho)$, given by

$$(\mu_{en}/\rho) = (\mu_K/\rho)(1-G) \tag{3}$$

The others are modifications of (2). In general, the last coefficients (2) and (3) are used to calculate the energy deposited in a material.

The mass attenuation coefficient, $\mu/\rho$, generally is used to calculate the reduction in flux density when passing through an absorbing material. It is this coefficient to which a buildup factor, $B_a$, must be applied in the form

$$\frac{D_t}{D_0} = B_a e^{-\mu t}$$

where $D_t$ is the dose after a shield thickness, $D_0$ is the dose before the shield and t is the thickness of the shield. The buildup factor, $B_a$, is the energy absorption buildup factor as defined in the reference by Kase and Nelson. Buildup factors for some materials were published by Goldstein and Wilkins,[10] and also may be found in the Engineering Compendium on Radiation Shielding.[11]

Transmission curves for 3 MeV photons in ordinary concrete as used in SPEAR are plotted in Fig. 3, using $(\mu/\rho)$ from Storm and Israel,[12] and the buildup factors for concrete. Also plotted on the same figure is the transmission curve without buildup, and the transmission curve using $(\mu_{en}/\rho)$.

There will be cases where the electromagnetic shower develops in materials other than lead, such as copper or iron used in flanges. The transmission curves, with and without buildup, of 8 MeV photons (the photon energy associated with copper or iron targets) in concrete is shown in Fig. 4. These curves agree with recent calculations and measurements of 8.2 MeV photons by Johnson et al.[13]

The references cited do not give buildup factors in concrete (or aluminum which may be considered as equivalent to concrete) for energies above 10 MeV. A buildup curve for 15 MeV, the energy of photons emerging from a thick aluminum target, was constructed by extrapolation of existing curves at lower energies, and is shown in Fig. 5. Using this build-up curve, the transmission curves in concrete for 15 MeV photons were constructed (see Fig. 6).

Transmission curves for 3 MeV photons in iron and in lead are shown as Fig. 7. Transmission curves for 8 MeV photons in iron are given in Fig. 8.

There is some question as to whether or not a buildup factor should be applied to photons emerging from a target struck by a high energy electron beam, where the shielding material is the same as the target material. (For these purposes, aluminum and concrete may be considered as equivalent.) The assumption is made here that whenever the target is truly a thick target (greater than shower maximum in length, and more than about 3 Molière units in radial dimensions), then all secondaries are in equilibrium, and no buildup factor need be applied. However, for thinner targets, this assumption is not made, and the buildup factor is applied.

Measurements

A report by DESY[14] has been published with which a comparison of the shielding of photons produced by a high energy beam may be made. Measurements were made of the transmission of photons through heavy concrete, with the photons produced by a 4.8 GeV bremsstrahlung beam incident upon a thick copper target. They measured

an attenuation coefficient of 0.065 $cm^{-1}$, or 0.0165 $cm^2/gm$. The average photon energy incident upon the heavy concrete shield from a copper target should be 8 MeV. Using a simplistic approach to the heavy concrete (assuming the concrete is 60% iron by weight, and 40% oxygen by weight), the attenuation coefficient was calculated to be 0.099 $cm^{-1}$ (DESY suggested a value of 0.090 $cm^{-1}$). Using 0.099 $cm^{-1}$ and the buildup factor for 8 MeV photons in iron, the curve of Fig. 9 was constructed. Again the calculated curve with buildup is more conservative than the measured value; however the agreement seems reasonable in light of the many simplifications made in constructing the curve.

III. Beam Incident upon a Thick Target at an Oblique Angle

The angular distribution of scattered ionizing radiation was reported in TN-70-34 for 2 GeV electrons obliquely incident upon a thick target. When the angle of incidence was zero, (i.e., the beam was targeting on the front face tangent to the inner edge of a collimator hole), attenuation measurements were made in lead of the scattered radiation at angles of 30 and 100 mradians as well as at $20^o$. The last angle was such that the scattered radiation passed through an extra five inches of iron, making these photons equivalent to 'thick target' photons in energy distribution. The photons at 30 and 100 mradians, however, would be those which emerged at shallow angles from the target, perhaps without having traversed much material.

The detectors were small capsules of LiF powder inserted in the lead bricks. The first capsule, mounted on the face of the lead, may indicate values lower than the other capsules simply due to the lack of electron equilibrium at that location. Electron equilibrium will be reached in a fraction of a radiation length. The second detector was located at a depth of 1.3 $X_0$ ($X_0$ = radiation length), with all other detectors at greater depths. Figure 10 shows the relative slopes of the attenuation curves in lead, which are the same as those measured previously from thick iron targets.[15] The measurements at 100 mradians and $20^o$ show only the slope corresponding to 8 MeV photons in lead. The first detector (taped to the face of the lead) reads higher at the larger angles which is interpreted to be due to the presence of many low energy electrons which are absorbed in the first few millimeters of lead, and which are not seen in the forward directions due to the greater number of high energy electrons. The 30 mradian measurement shows a buildup which reaches a maximum at around 2.7 $X_0$.

Measurements also were made with the beam striking the inner face of the collimator at oblique angles of $3^{o}$ and $9^{o}$. Measurements were made in lead at scattering angles of $6^{o}$ and $20^{o}$. No buildup was observed at either scattering angle, except for the expected rise between the first and second detectors.

One interpretation of Fig. 10 is that a maximum photon energy may be ascribed to the scattered radiation as a function of the scattering angle. For the case of the beam tangent to the inner face, the buildup reached a maximum at $2.7\ X_0$. According to Rossi,[16] Approximation B of shower theory would predict an optimum thickness for photons to be $\sim 1.1\ (\ell n\ E_0/\epsilon_0 - 1)$ where $\epsilon_0$ is the critical energy for the target material. For lead, $\epsilon_0 = 7.5$ MeV. Then the energy associated with an optimum thickness of $2.7\ X_0$ would be

$$2.7 = 1.1\left(\ell n\ \frac{E_0}{7.5} - 1\right)$$

$$E_0 \cong 240 \text{ MeV} \quad .$$

For all other scattering angles, no buildup was observed, and the assumption is made that the average photon energy is that associated with the minimum in the attenuation coefficient. This holds for all angles greater than 100 mradians. Angles less than 100 mradians must be treated as having a higher energy component.

IV. Beam Incident at Oblique Angles on a Thin Aluminum Target

The angular distribution of radiation scattered from a 1/4 inch aluminum plate struck by a 2 GeV electron beam at an angle of $4^{o}$ was reported in TN-70-34. The assignment of an average photon energy is not as simple as in the case of a thick target, however. The beam, through the 1/4" thick plate at $4^{o}$ will traverse about 9 cm, or $1\ X_0$ in the beam direction, before emerging. The radial dimensions are always less than 0.03 Moliere units, where a Molière unit, which is the characteristic measure for radial distributions in shower theory, is given as $X_0 E_s/\epsilon_0$, where $E_s = 21.2$ MeV and $\epsilon_0$ is the critical energy of the material. From radial losses alone, it is evident that almost all the energy will escape from the aluminum plate.

Unfortunately no experimental evidence exists for determining the energy of the scattered radiation as a function of scattering angle. In TN-70-34, multiple scattering of the primary electron beam was examined as a possible source of

the radiation measured beyond $15^{o}$. This was ruled out using Moliere scattering theory[17] which was modified further from experimental work at SLAC to account for a finite beam shape.[18] At $15^{o}$, the calculated value would be about 4 rad - $m^2/10^{13}$ $e^-$, while the measured value was 150 rad - $m^2/10^{13}$ $e^-$.

Delta rays were postulated by DeStaebler as one source of the large 'tail' in the measurements. These would have a maximum energy of 2 MeV.

For SPEAR, all photons at angles up to $15^{o}$ are assumed to have high energies (up to $E_0$), while the energy of the minimum of the attenuation coefficient is assigned to all photons beyond $15^{o}$. Also, because of the uncertainty in energy, the buildup factor for 15 MeV photons is used for the thin target case in order to give conservative numbers in the shielding design.

## V. Transmission of Photons Incident upon Concrete at Oblique Angles

The previous sections have dealt with the transmission of photons through finite shields assuming that the photons are unidirectional and normal to the shield. Such is not always the case, especially for SPEAR which is a circular machine. The intensity of radiation normal to the shield (which also is produced at an angle of $90^{o}$ to the beam) may be significantly lower than the intensity in forward directions, as shown in TN-70-34. It would be incorrect simply to apply the attenuation through the slant range of the shield to determine transmission. Many photons will scatter out of the shield at large angles having traversed less material than in the slant direction.

The discussion that follows, draws heavily upon the work of W. O. Doggett and F. A. Bryan, Jr.[19] who performed a Monte Carlo analysis for dose transmission of plane unidirectional photons with energies between 0.2 and 10 MeV. They give curves for transmission at various angles of incidence, $\theta$, with the dose calculated at a detector position as shown in the sketch.

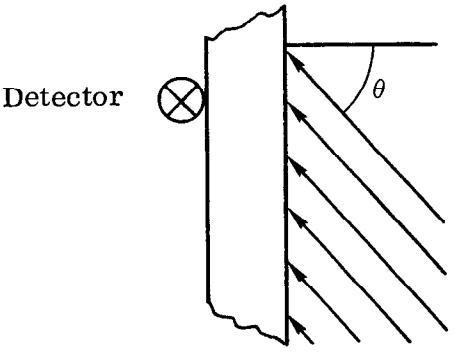

Transmission curves are given for various photon energies, including 1.25, 5 and 10 MeV. The 10 MeV data, shown in Fig. 11, is used for photons with energies near the attenuation minimum for aluminum. For 3 MeV photons from lead, which is of considerable interest to SPEAR, the data between 1.25 and 5 MeV was extrapolated in a linear fashion, and the 3 MeV curves of Fig. 12 drawn.

Using Figs. 11 and 12, the transmission through 2 feet of concrete of 3 MeV and 10 MeV photons was calculated; also the transmission of 10 MeV photons through 3 feet of concrete for the different angles of incidence. These are shown as Fig. 13.

VI. Photon Doses Inside a Ring Source

The geometry of a source distributed uniformly around a ring is shown in the following figure.

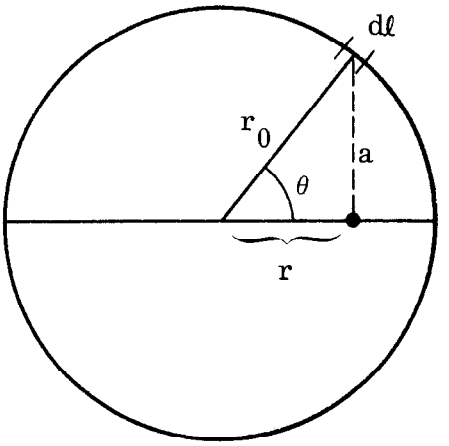


$$a^2 = r_0^2 + r^2 - 2r_0 r \cos\theta$$

If we make the assumption that the source radiates isotropically, the problem is greatly simplified. For the dose distributions from thick targets as given in TN-70-34, this is true to a factor of $\sim 3$ for angles greater than $30^{\circ}$. Then, the dose from a segment, $d\ell$, at a point, r, inside the ring may be calculated quite easily. We use the dose, $D_0$, measured from a point source at some distance, R, to calculate the source strength, Q

$$Q = \frac{D_0 R^2 4\pi}{f} \quad ,$$

where f is the conversion factor from flux to dose. The dose inside a ring at a distance, r, from the center coming from an element, $d\ell$ (where $d\ell = r_0 d\theta$) of a

source distributed around a circumference, $c = 2\pi r_0$, is

$$dD = \frac{fQ}{4\pi a^2} \frac{d\ell}{c}$$

$$= \frac{f\,4\pi\,D_0 R^2}{f\,4\pi a^2} \frac{d\ell}{c}$$

$$= \frac{D_0 R^2}{a^2} \frac{r_0\,d\theta}{2\pi r_0}$$

$$= \frac{D_0 R^2}{2\pi a^2}\,d\theta$$

Integrating this expression will give the total dose from the ring.

$$D = \frac{D_0 R^2}{2\pi} \int_0^{2\pi} \frac{d\theta}{r_0^2 + r^2 - 2r_0 r \cos\theta}$$

The dose will be symmetric from each half of the ring, giving

$$D = \frac{D_0 R^2}{\pi} \int_0^{\pi} \frac{d\theta}{r_0^2 + r^2 - 2r_0 r \cos\theta}$$

$$= \frac{D_0 R^2}{\left| r_0^2 - r^2 \right|} \qquad (1)$$

For the case of a shield between the ring and the point of measurement, the problems becomes more complicated because the shield does not present a constant thickness to any point inside the ring except the very center. At r=0, the dose will be

$$D = B\,e^{-\mu t} \frac{D_0 R^2}{\left| r_0^2 - r^2 \right|} \qquad (2)$$

For all other locations, both the buildup factor and the transmission given by $e^{-\mu t}$ are functions of the angle, $\theta$; that is

$$D = \frac{D_0 R^2}{\pi} \int_0^{\pi} \frac{B(t(\theta))\, e^{-\mu t(\theta)}\, d\theta}{r_0^2 + r^2 - 2 r_0 r \cos\theta} \quad . \tag{3}$$

The thickness, t, may be related to $\theta$ in various trigonometric ways, one of which is presented here (courtesy of K. Kase).

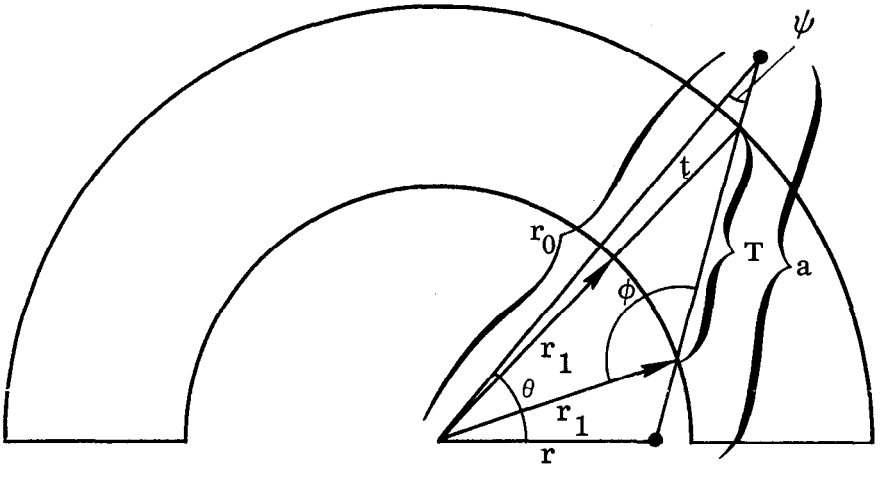


$$T^2 + r_1^2 - 2 T r_1 \cos\phi = (r_1 + t)^2$$

where t is the nominal thickness of the shield and T is the slant thickness. Then using trigonometric identities

$$\frac{r_0}{\sin\phi} = \frac{r_1}{\sin\psi} \qquad \text{and} \qquad \frac{r}{\sin\psi} = \frac{a}{\sin\theta}$$

we get

$$\frac{r_1 \sin\phi}{r_0} = \frac{r \sin\theta}{a} \quad ,$$

$$\sin\phi = \frac{r_0 r}{r_1 a} \sin\theta \quad , \cdot$$

and

$$\cos \phi = (1 - \sin^2 \phi)^{1/2} = \left[1 - \left(\frac{r_0 r}{r_1^a}\right)^2 \sin^2 \theta\right]^{1/2} .$$

The solution of the integral is trivial if one has a computer at hand. The results are shown in Fig. 14 for shield thicknesses of 2 and 3 feet. Also included is a curve using a constant shield thickness (not a function of $\theta$) as in expression (2), which is accurate only at the center of the ring. Using expression (2) overestimates the doses near the shield by as much as a factor of 4.

Acknowledgements

The author wishes to express thanks to H. DeStaebler, W. R. Nelson and K. Kase for helpful discussions, and to D. Peckham for help in preparing the figures.

## References


1. H. DeStaebler, Jr., "Transverse shielding for the Stanford two-mile accelerator," Report No. SLAC-9 (1962), and many others.
2. W. S. Gilbert et al., "1966 CERN-LRL-RHEL shielding experiment at the CERN Proton Synchrotron," Report No. UCRL-17941 (1968).
3. T. M. Jenkins et al., "Angular distribution of radiation from a collimator, a thick plate and a thin plate struck by a 2 GeV electron beam," Report No. SLAC-TN-70-34 (1970).
4. J. L. Harris and T. M. Jenkins, "Shielding of SPEAR," SPEAR-21 (1971) (internal document).
5. S. Glasstone and A. Sesonske, Nuclear Reactor Engineering (D. Van Nostrand Co., Inc., Princeton, N.J., 1955).
6. B. T. Price, C. C. Horton and K. T. Spinney, Radiation Shielding, (The Macmillan Co., New York, 1957).
7. W. R. Nelson et al., "Electron-induced cascade showers in copper and lead at 1 GeV," Phys. Rev. 149 (1966).
8. H. H. Nagel, "Electron-photon cascade showers in lead," Z. Physik. 186 (1965).
9. K. Kase and W. R. Nelson, "Notes on radiation dosimetry," to be published.
10. H. Goldstein and J. E. Wilkins, Jr., USAEC Report NYO-3075.
11. R. G. Jaeger, ed., Engineering Compendium on Radiation Shielding, Vol. I (Springer-Verlag, New York, 1968).
12. E. Storm and H. I. Israel, "Photon cross sections from 0.001 to 100 MeV for elements 1 through 100," Report No. LA-3753 (1967).
13. W. R. Johnson et al., "Gamma-ray attenuation at energies of approximately 6 and 8 MeV," Nucl. Sci. and Eng. 43 (1971).
14. G. Bathow et al., "Shielding measurements on 4.8 GeV bremsstrahlung," Nucl. Instr. Methods 33 (1965).
15. R. B. Neal, ed., The Stanford Two-Mile Accelerator, (Benjamin, New York, 1968) Chapter 26.
16. B. Rossi, High-Energy Physics (Prentice-Hall, Inc., Englewood Cliff, N.J., 1952).
17. J. B. Marion and B. A. Zimmerman, "Multiple scattering of charged particles," Nucl. Instr. Methods 51 (1967).

18. T. M. Jenkins and W. R. Nelson, "The effect of target scattering on the shielding of high energy electron beams," Health Phys. 17 (1969).

19. W. O. Doggett and F. A. Bryan, Jr., "Theoretical dose transmission and reflection probabilities for 0.2 - 10 MeV photons obliquely incident on finite concrete barriers," Nucl. Sci. and Eng. 30 (1970).

## Figure Captions

1. Relative photon energy distribution in lead at a depth of 7 shower maxima (from Ref. 8).
2. Transmission of the photon spectrum of Fig. 1 in concrete. Curve A — transmission of 3 MeV photons with buildup. Curve C — transmission of 3 MeV photons without buildup. Curve B — dividing the spectrum into energy intervals and using the buildup for each energy interval.
3. Transmission of 3 MeV photons through ordinary concrete. Curve A — using $(\mu_{en}/\rho)$ used to calculate energy absorbed in the shield. Curve B — using $(\mu/\rho)$ with buildup. Curve C — using $(\mu/\rho)$ without buildup.
4. Transmission of 8 MeV photons in ordinary concrete. Curve A — with buildup. Curve B — without buildup.
5. Energy absorption buildup factors in concrete from Ref. 11. The 15 MeV curve is an extrapolation.
6. Transmission of 15 MeV photons through concrete. Curve A — using $(\mu_{en}/\rho)$. Curve B — using $(\mu/\rho)$ with the buildup of Fig. 5. Curve C — using $(\mu/\rho)$ without buildup.
7. Transmission of 3 MeV photons. Curves A and B — transmission through iron with and without buildup. Curves C and D — transmission through lead with and without buildup.
8. Transmission of 8 MeV photons through iron, with (curve A) and without (curve B) buildup.
9. Comparison of calculations with measurement of transmission through heavy concrete at DESY. The buildup for iron was used for curve A. Curve C — without buildup. Curve B — DESY measurement.
10. Transmission of photons in lead from an iron target. Only the 30 mradian curve (beam on edge) shows a buildup. The slopes (solid lines) correspond to $(\mu/\rho)$ for 8 MeV photons in lead.
11. Dose transmission probability for 10 MeV plane unidirectional photons on concrete (from Ref. 18). The values beyond 4 mean-free paths are extrapolated.
12. Dose transmission probability for 3 MeV plane unidirectional photons on concrete (extrapolated from Ref. 18). The values beyond 4 mean-free paths are extrapolated.

13. Transmission of plane unidirectional 3 and 10 MeV photons through concrete. Curve A — 10 MeV photons through 2' thick concrete. Curve B — 3 MeV photons through 2' thick concrete. Curve C — 10 MeV photons through 3' thick concrete.
14. Doses per $10^{13}$ electrons inside a 30 meter storage ring assuming an isotropic 80 rads per $10^{13}$ electrons at 1 meter for a point source. Doses for 2 and 3 foot thick shields are shown calculated by Eq. (2) and by Eq. (3).

Figure 1

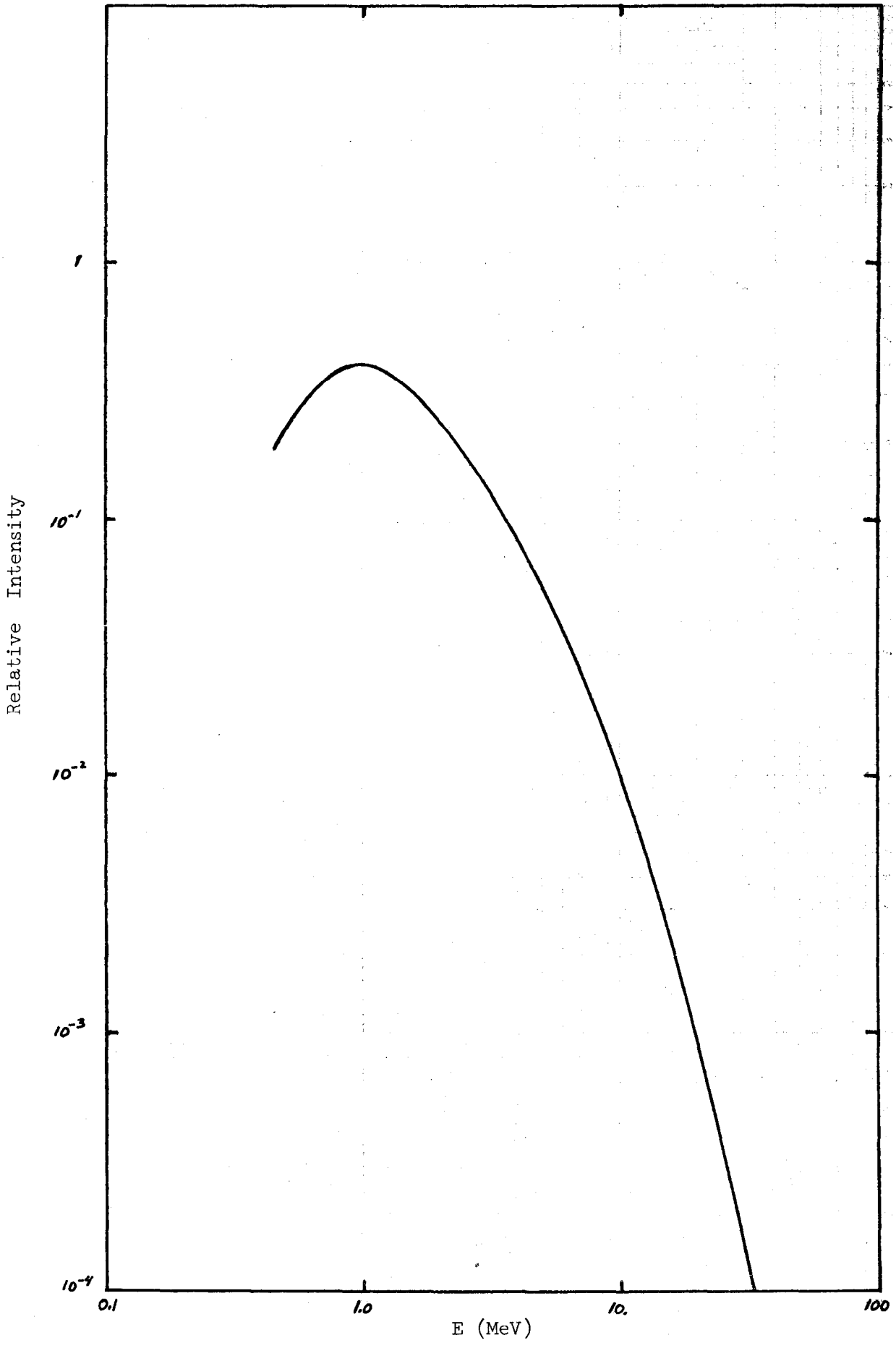

Figure 2

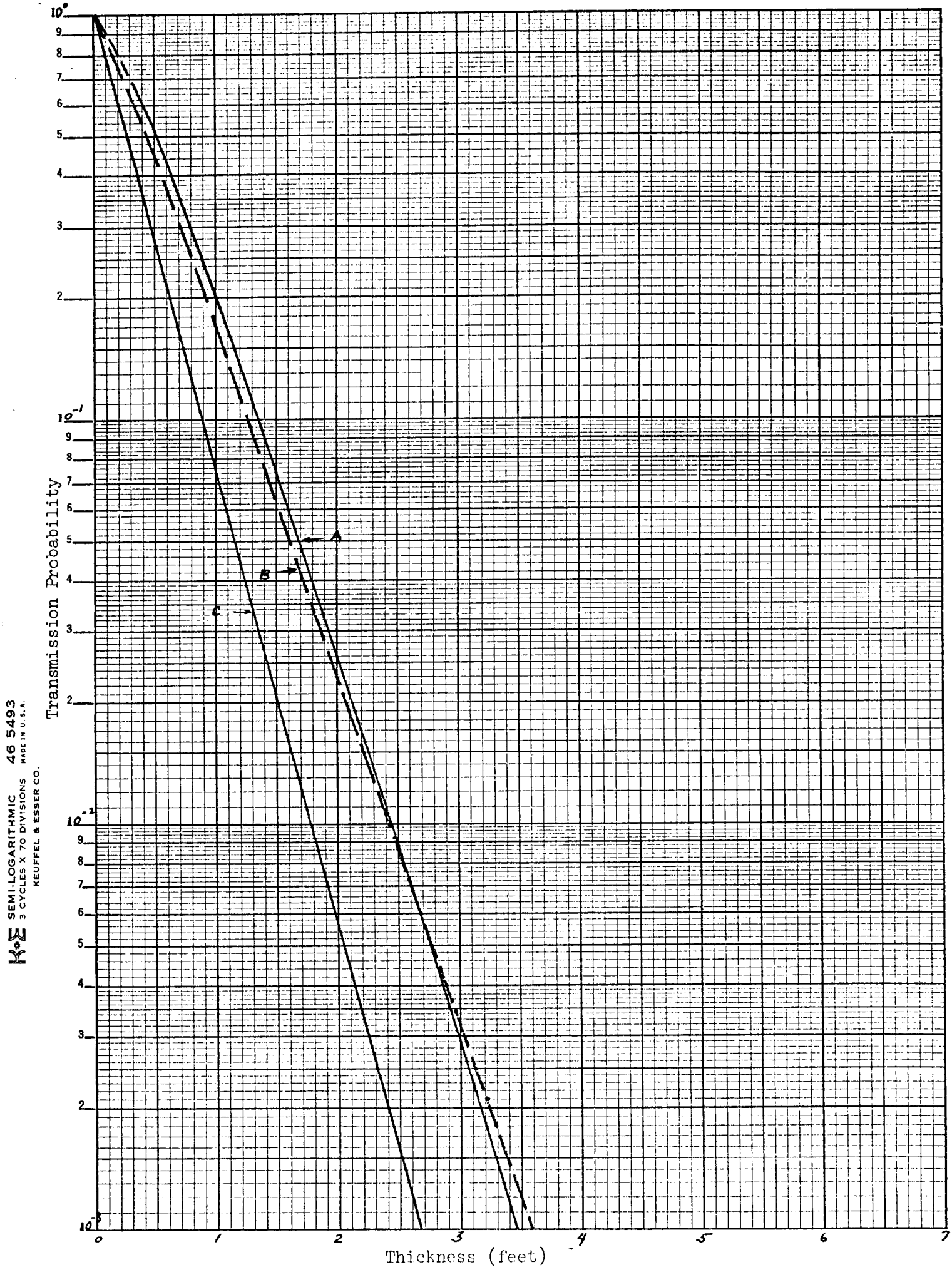
Transmission Probability
Thickness (feet)
A
B
C
SEMI-LOGARITHMIC 46 5493
3 CYCLES X 70 DIVISIONS MADE IN U.S.A.
KEUFFEL & ESSER CO.

Figure 3

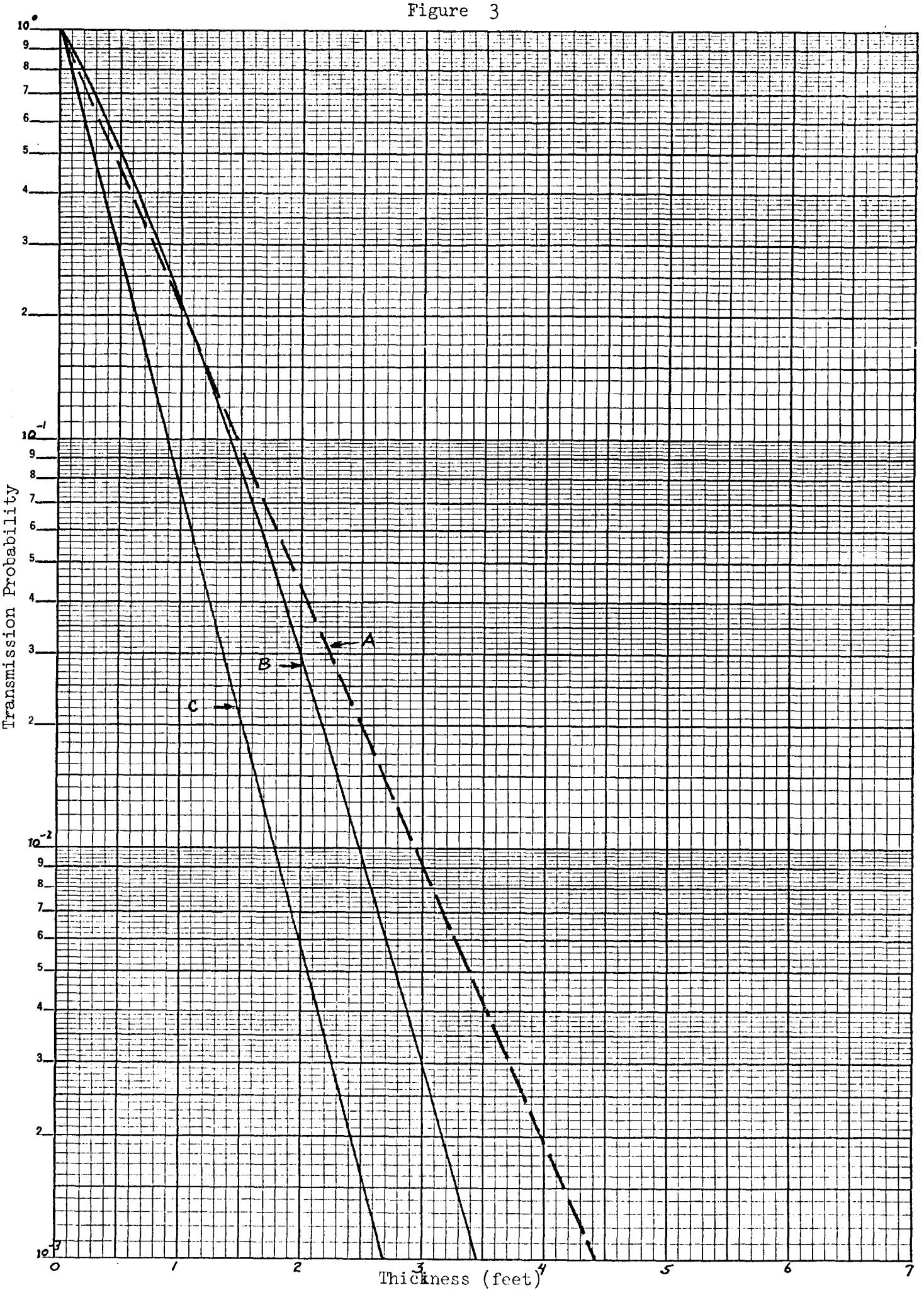
Transmission Probability
Thickness (feet)
A
B
C
0
1
2
3
4
5
6
7
SEMI-LOGARITHMIC 46 5493
3 CYCLES X 70 DIVISIONS MADE IN U.S.A.
KEUFFEL & ESSER CO.

Figure 4

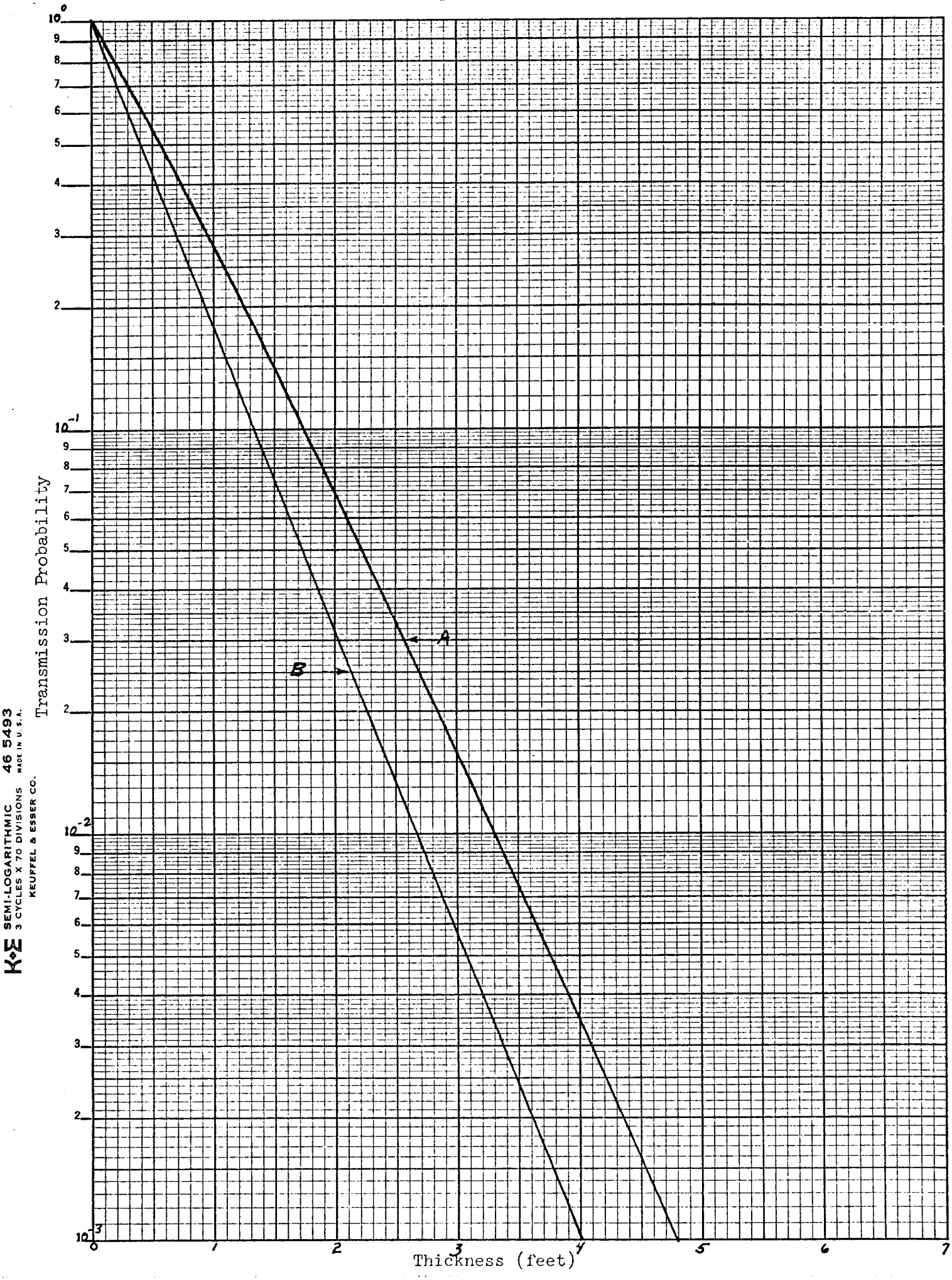
Transmission Probability
$10^{0}$
9
8
7
6
5
4
3
2
$10^{-1}$
9
8
7
6
5
4
3
2
$10^{-2}$
9
8
7
6
5
4
3
2
$10^{-3}$
A
B
0
1
2
3
4
5
6
7
Thickness (feet)
K&E SEMI-LOGARITHMIC 46 5493
3 CYCLES X 70 DIVISIONS MADE IN U.S.A.
KEUFFEL & ESSER CO.

Figure 5

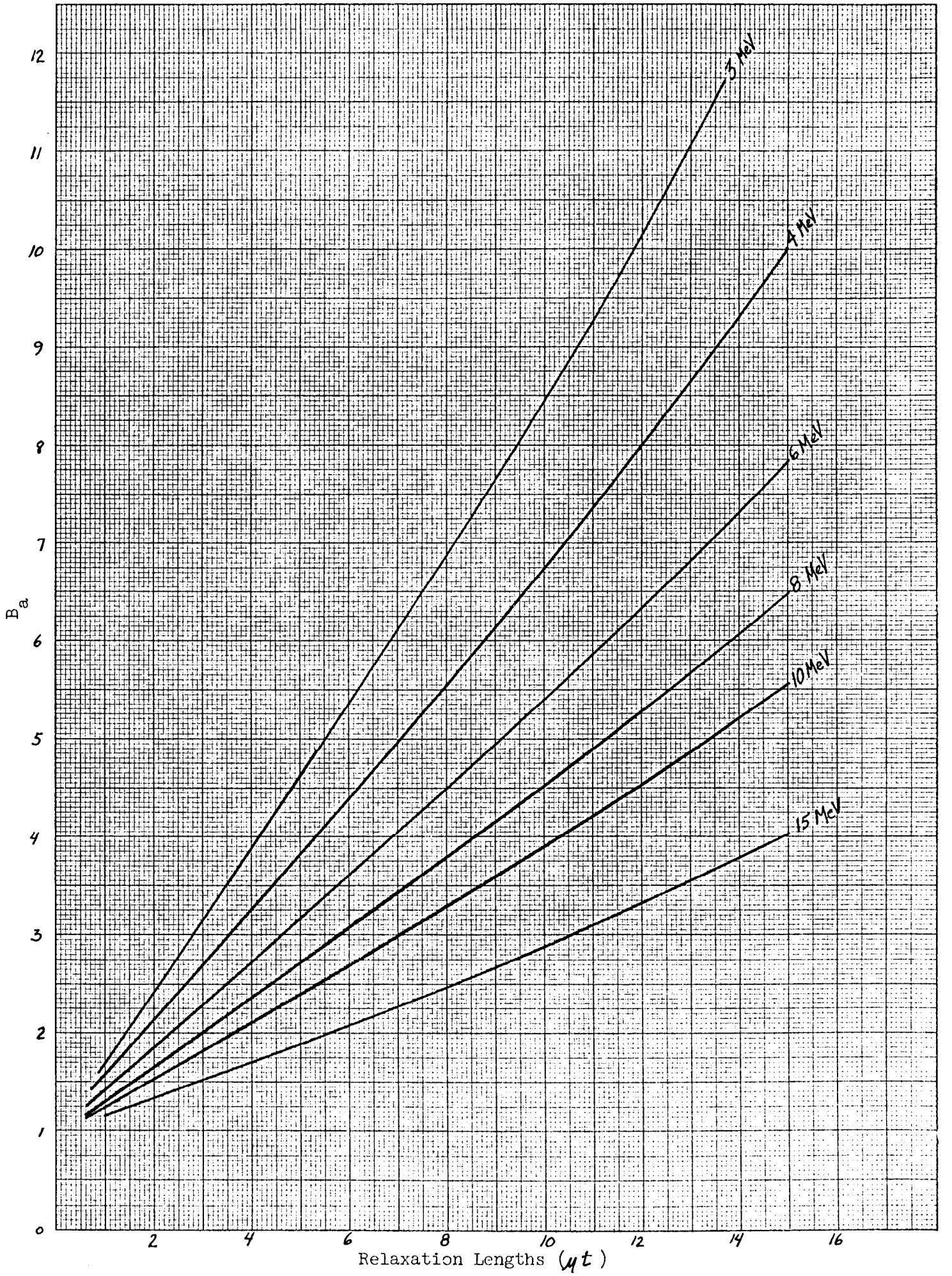

Figure 6

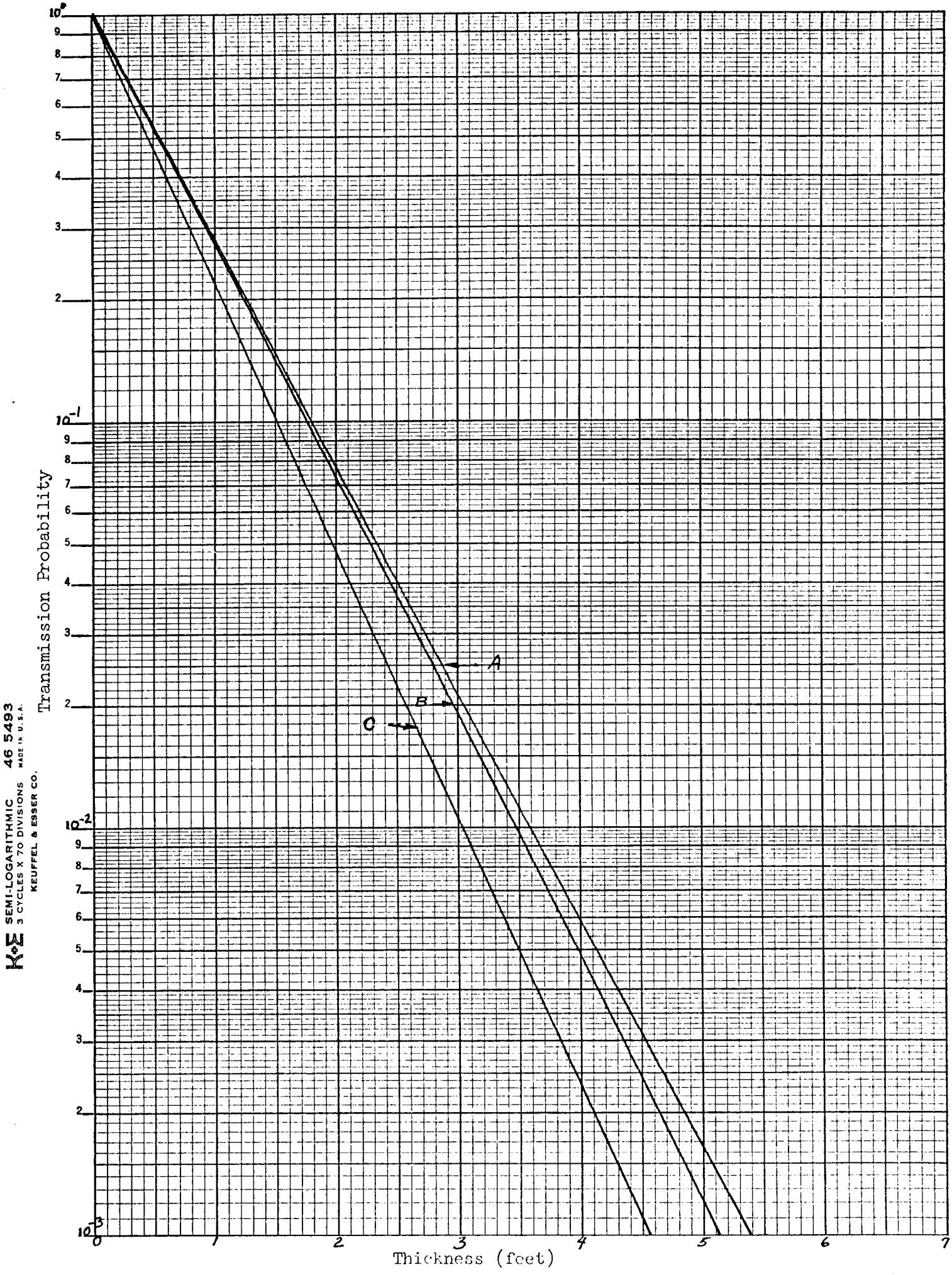
Transmission Probability
Thickness (feet)
A
B
C
SEMI-LOGARITHMIC
3 CYCLES X 70 DIVISIONS
KEUFFEL & ESSER CO.
46 5493
MADE IN U.S.A.

Figure 7

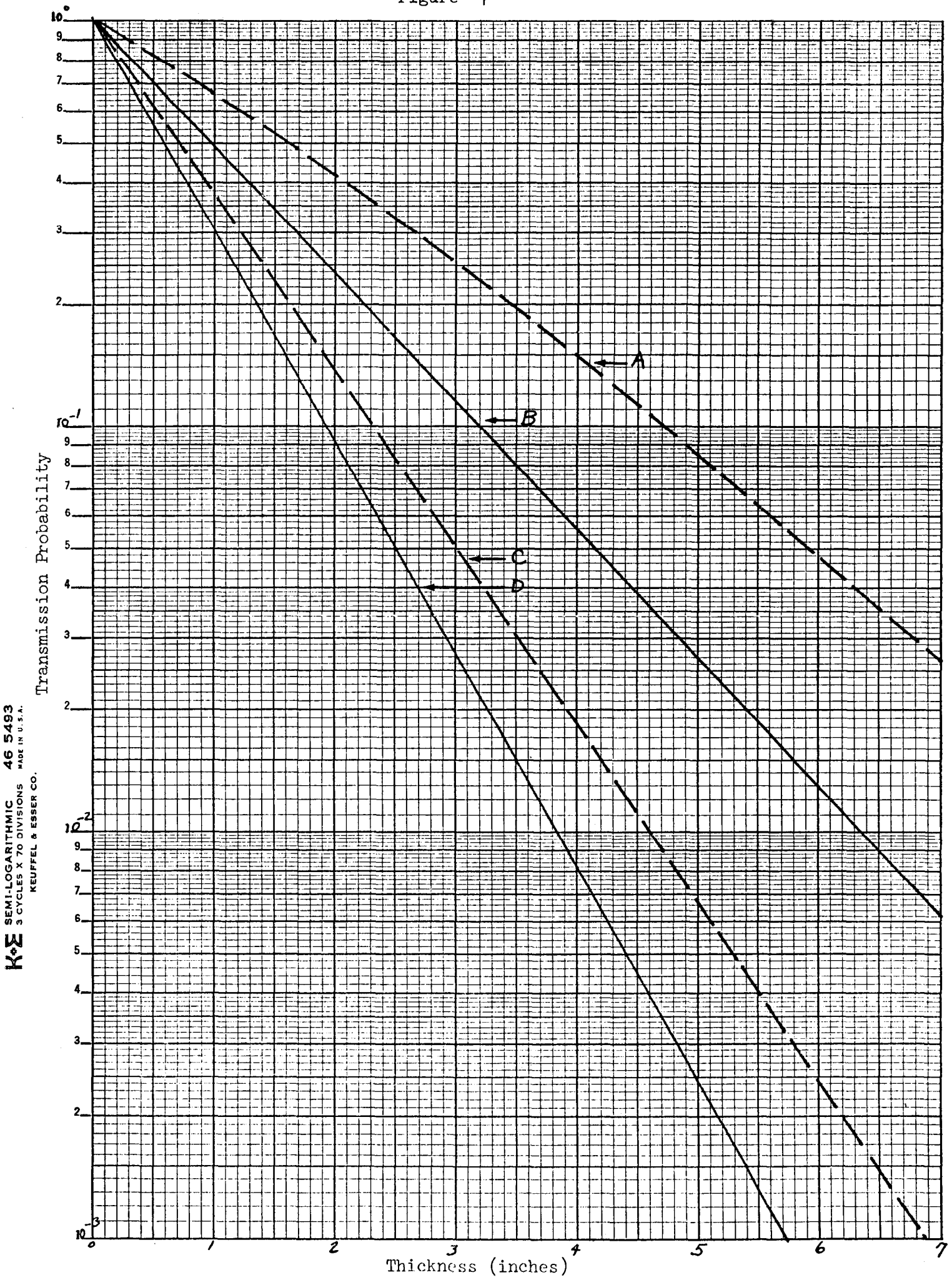
Transmission Probability
Thickness (inches)
A
B
C
D
0
1
2
3
4
5
6
7
SEMI-LOGARITHMIC 46 5493
3 CYCLES X 70 DIVISIONS MADE IN U.S.A.
KEUFFEL & ESSER CO.

Figure 8

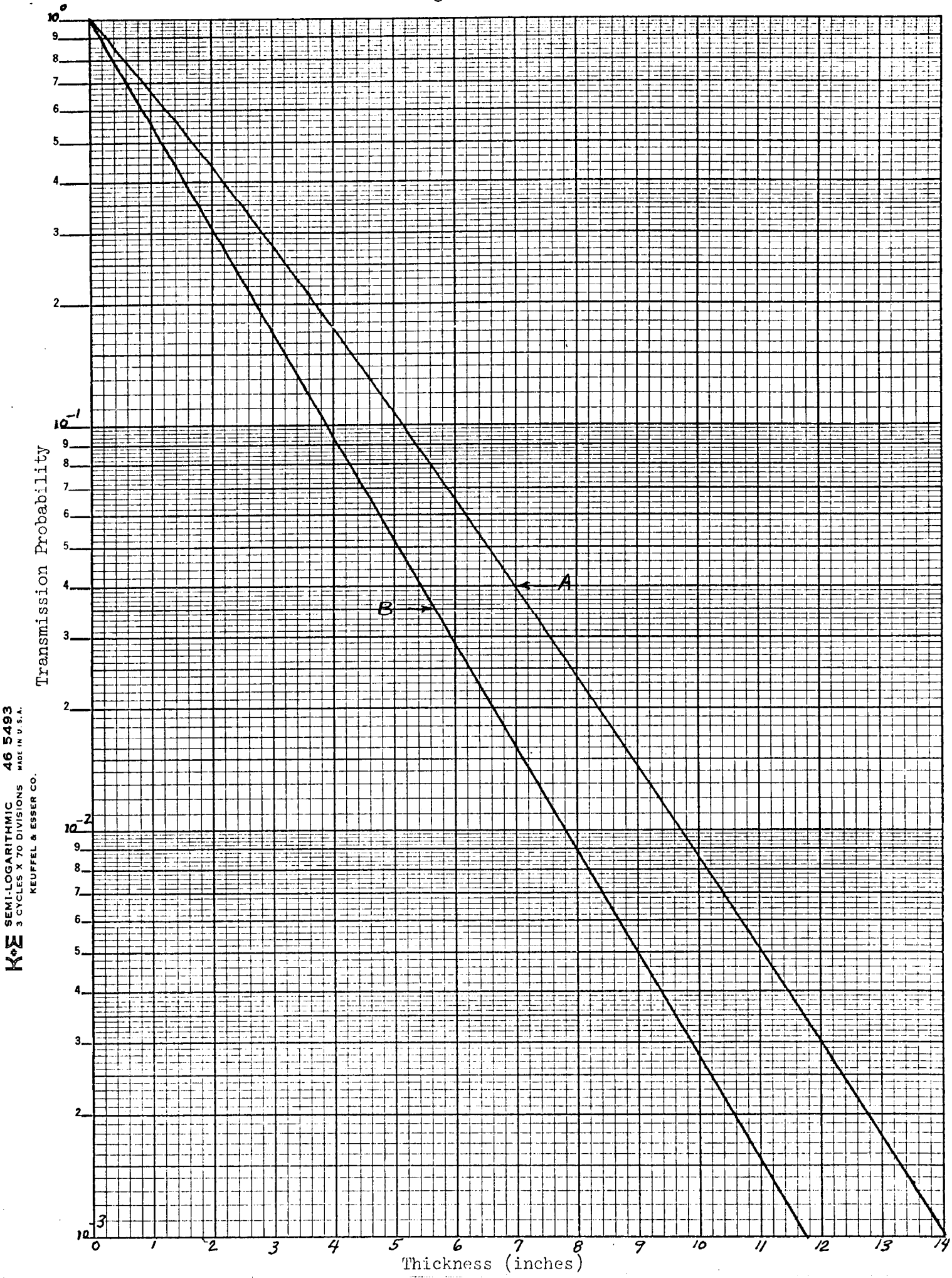
Transmission Probability
Thickness (inches)
A
B
SEMI-LOGARITHMIC 46 5493
3 CYCLES X 70 DIVISIONS MADE IN U.S.A.
KEUFFEL & ESSER CO.

Figure 9

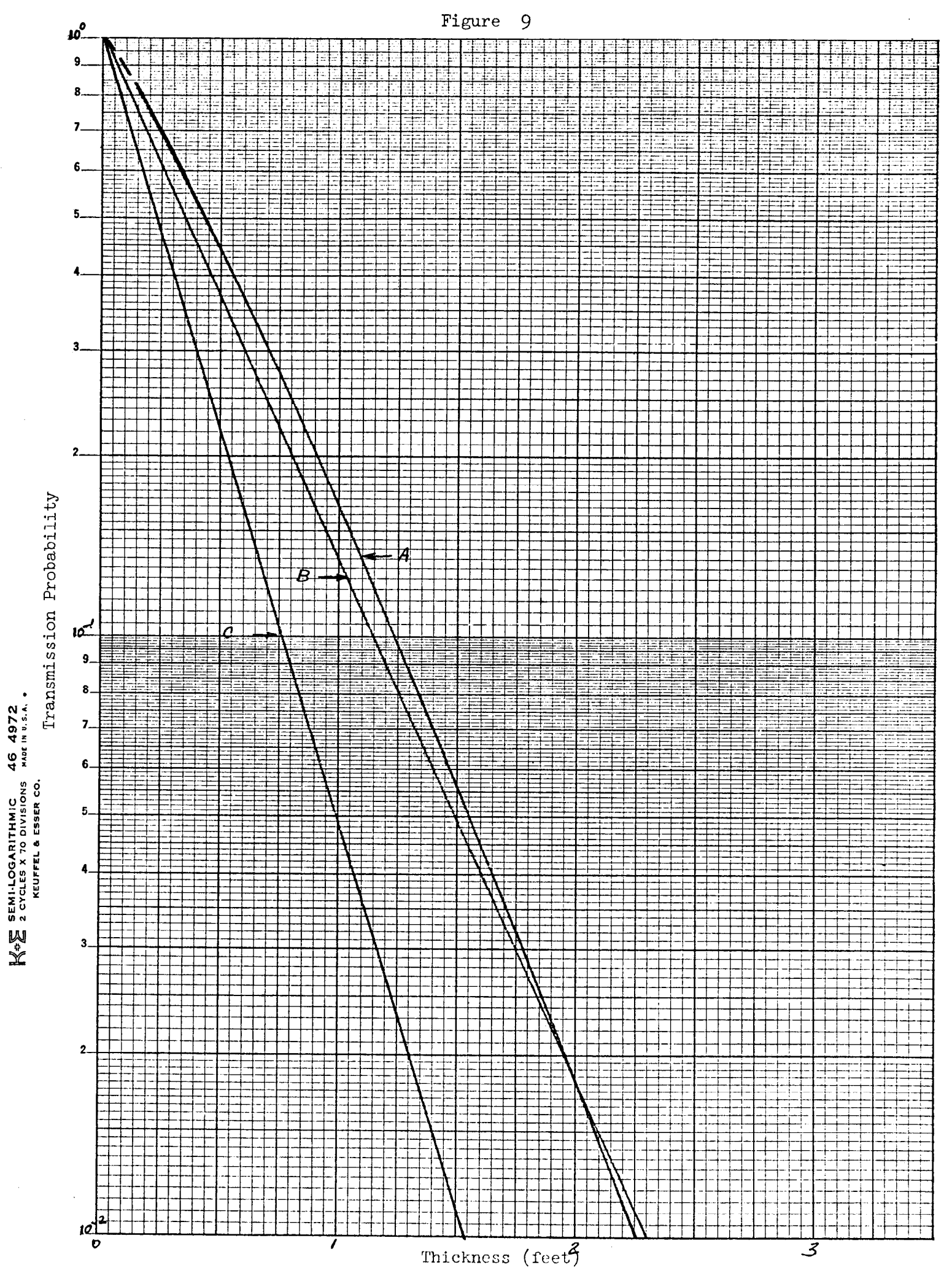
Transmission Probability
Thickness (feet)
A
B
C
$10^0$
$10^{-1}$
$10^{-2}$
0
1
2
3
SEMI-LOGARITHMIC 46 4972
2 CYCLES X 70 DIVISIONS MADE IN U.S.A.
KEUFFEL & ESSER CO.

Figure 10

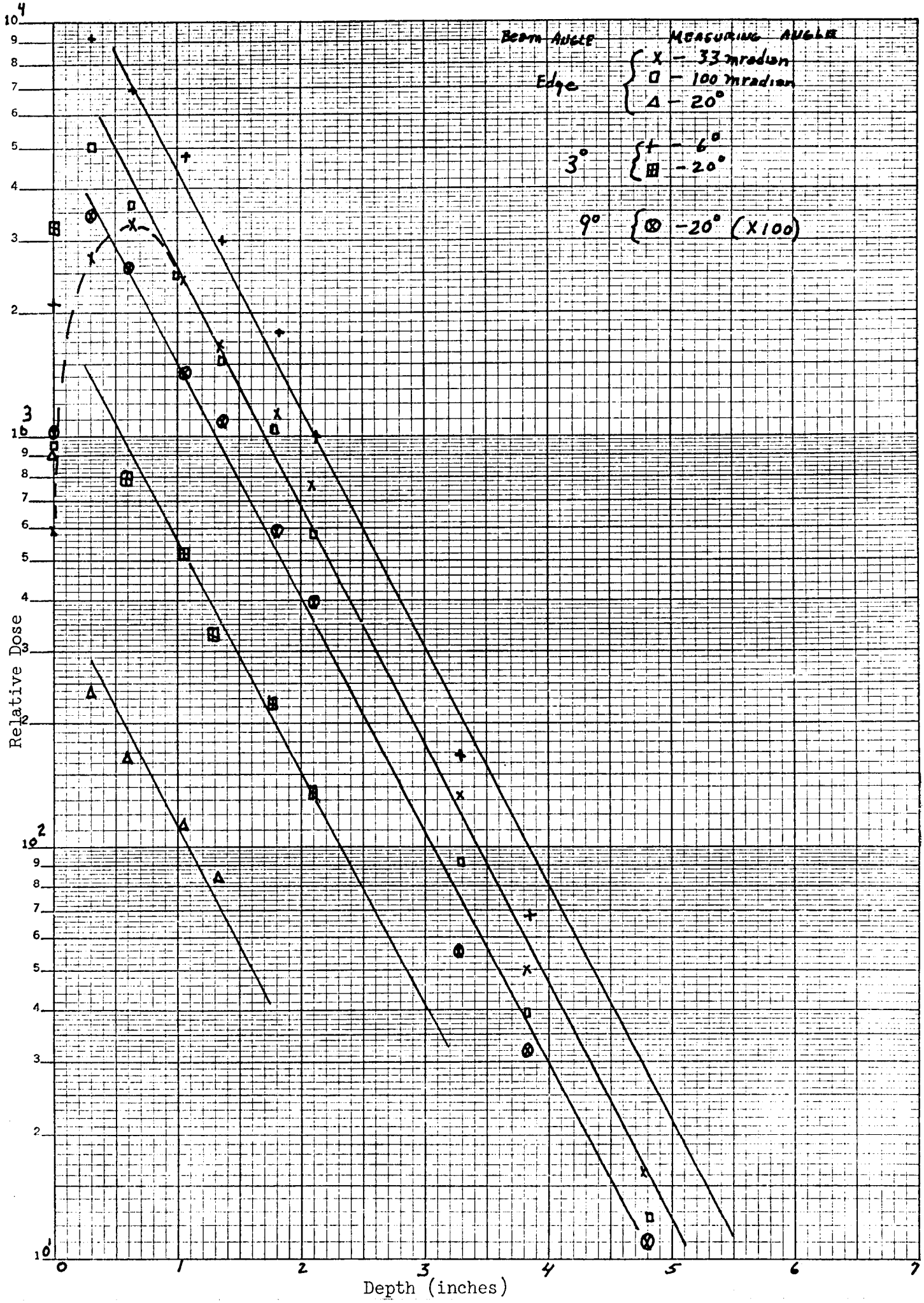
Beam Angle
Edge
Measuring Angle
X – 33 mradian
□ – 100 mradian
Δ – 20°
3°
+ – 6°
⊞ – 20°
9°
⊗ – 20° (X100)
Relative Dose
Depth (inches)
SEMI-LOGARITHMIC
3 CYCLES X 70 DIVISIONS
KEUFFEL & ESSER CO.
46 5492
MADE IN U.S.A.

Figure 11

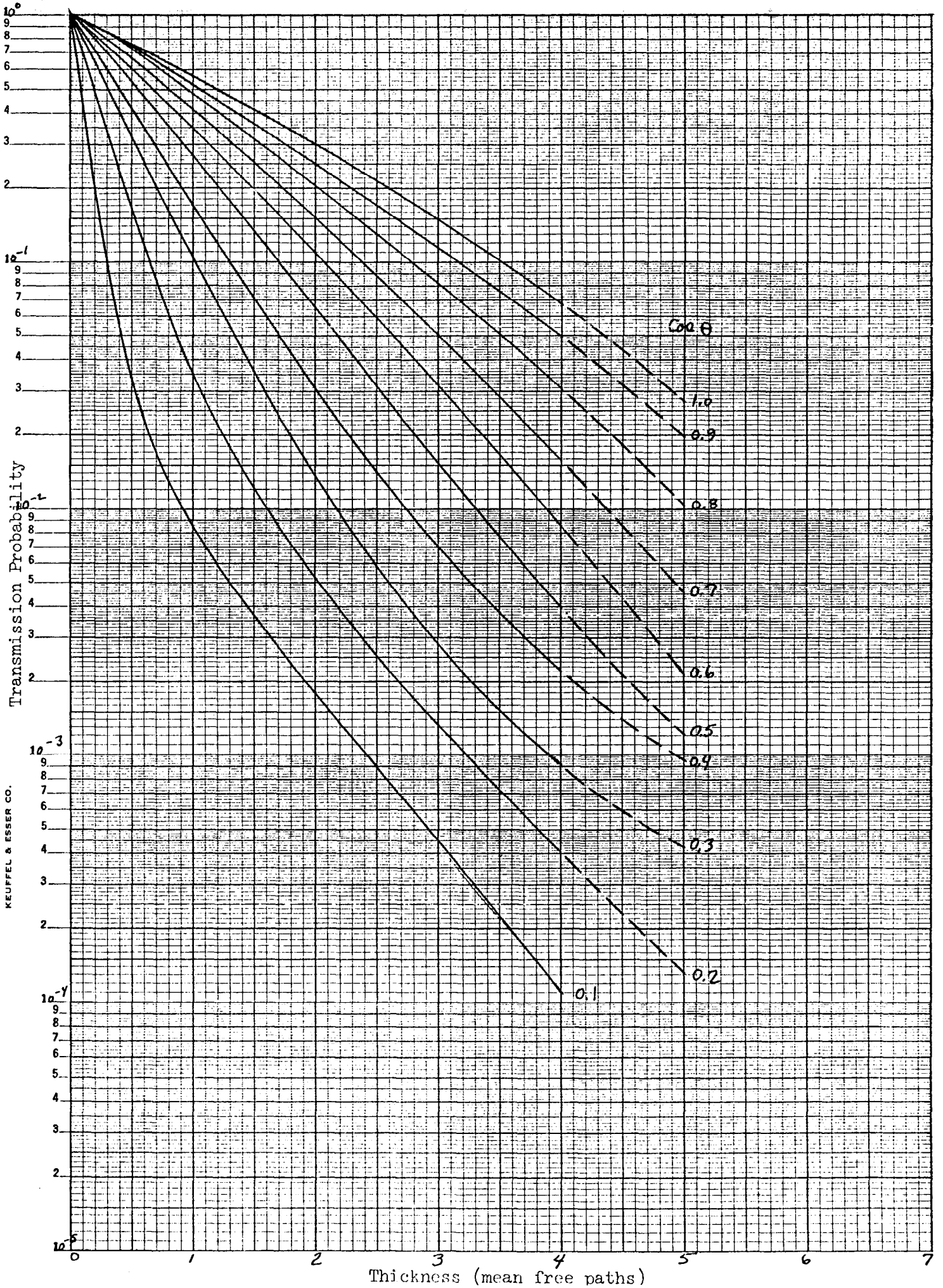
Transmission Probability
Thickness (mean free paths)
Cos θ
1.0
0.9
0.8
0.7
0.6
0.5
0.4
0.3
0.2
0.1
0
1
2
3
4
5
6
7
SEMI-LOGARITHMIC
5 CYCLES X 70 DIVISIONS
KEUFFEL & ESSER CO.
MADE IN U.S.A.
46 6212

Figure 12

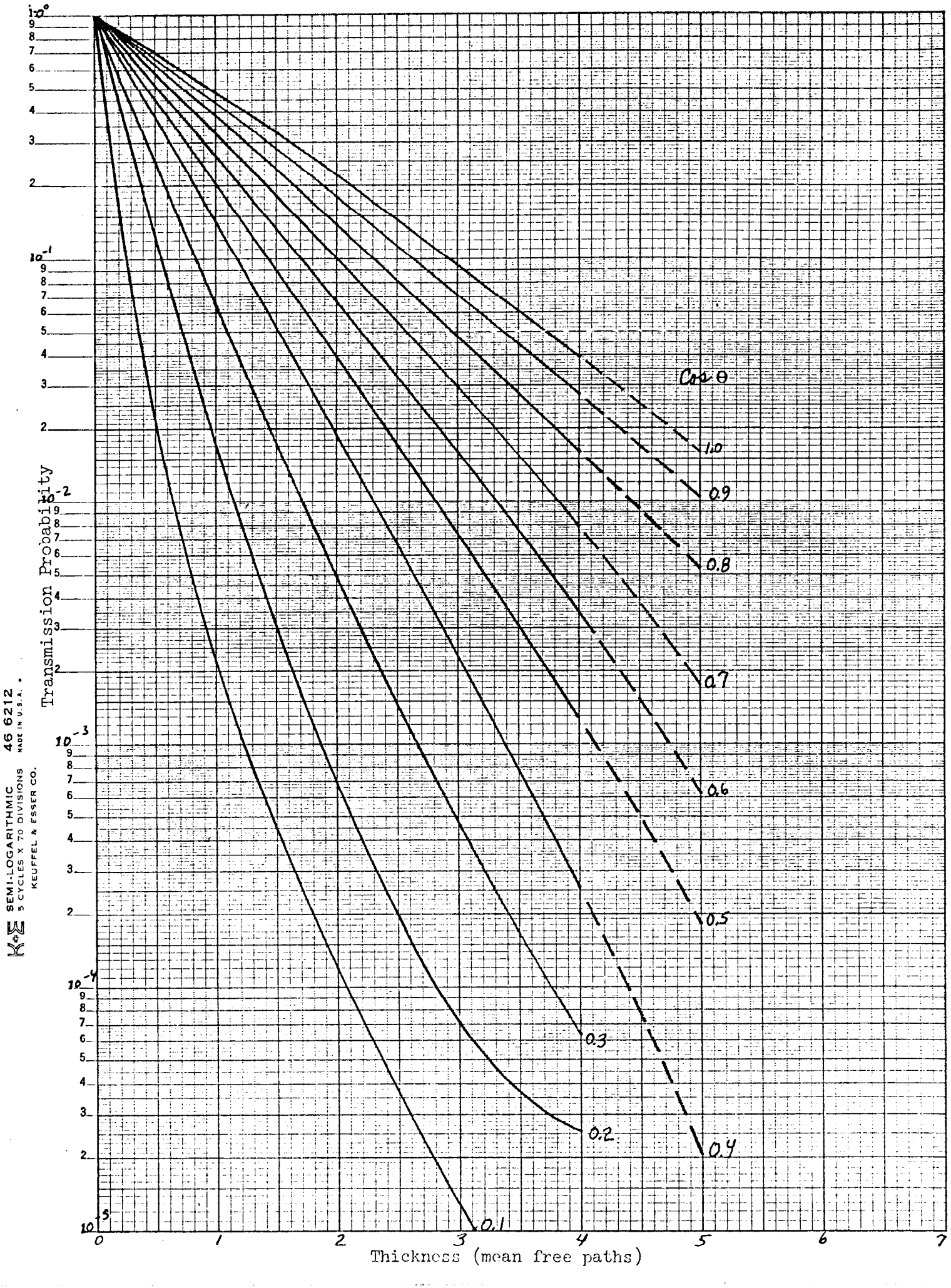
Transmission Probability
Thickness (mean free paths)
Cos θ
1.0
0.9
0.8
0.7
0.6
0.5
0.4
0.3
0.2
0.1
SEMI-LOGARITHMIC
5 CYCLES X 70 DIVISIONS
KEUFFEL & ESSER CO.
46 6212
MADE IN U.S.A.

Figure 13

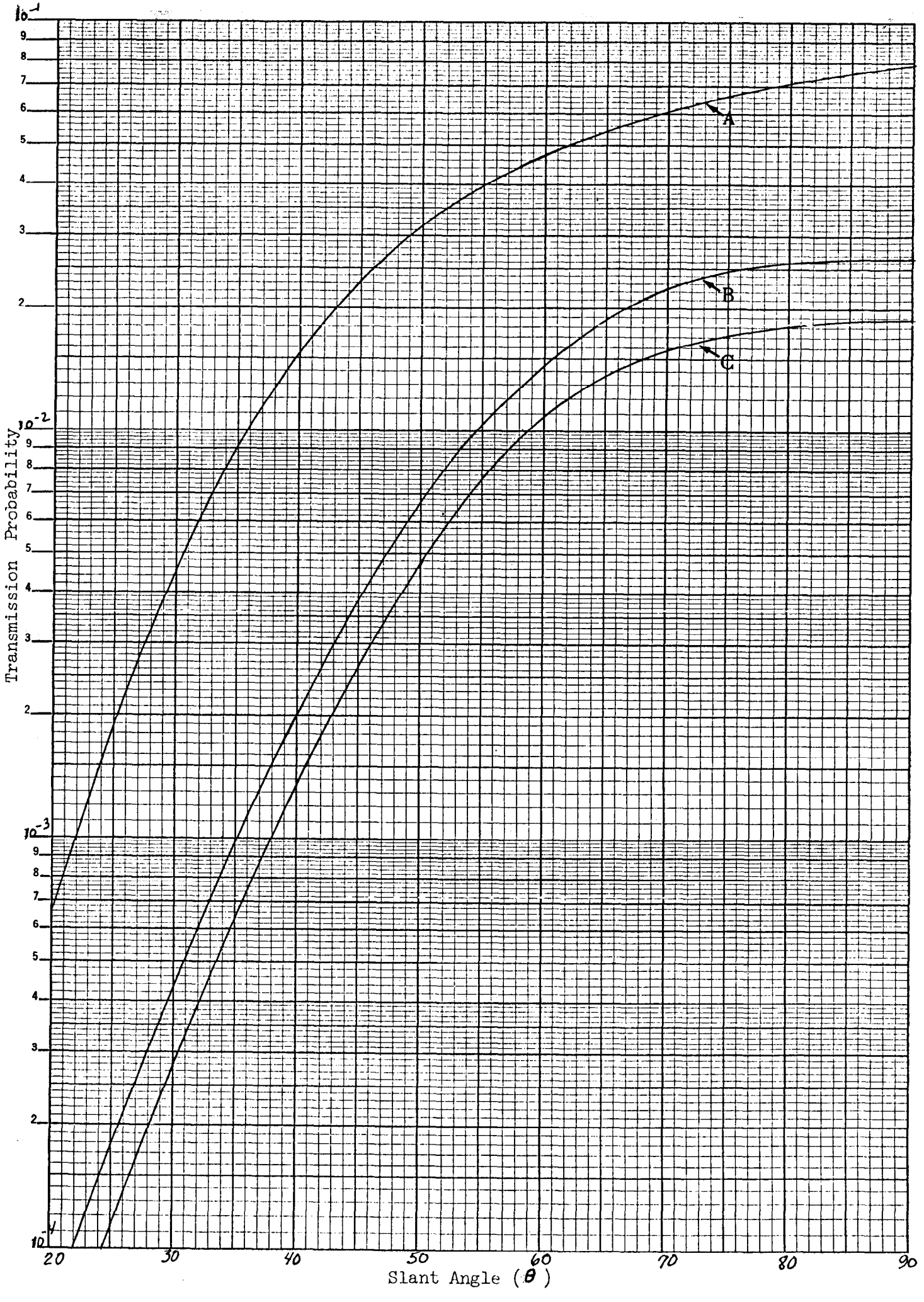

Figure 14

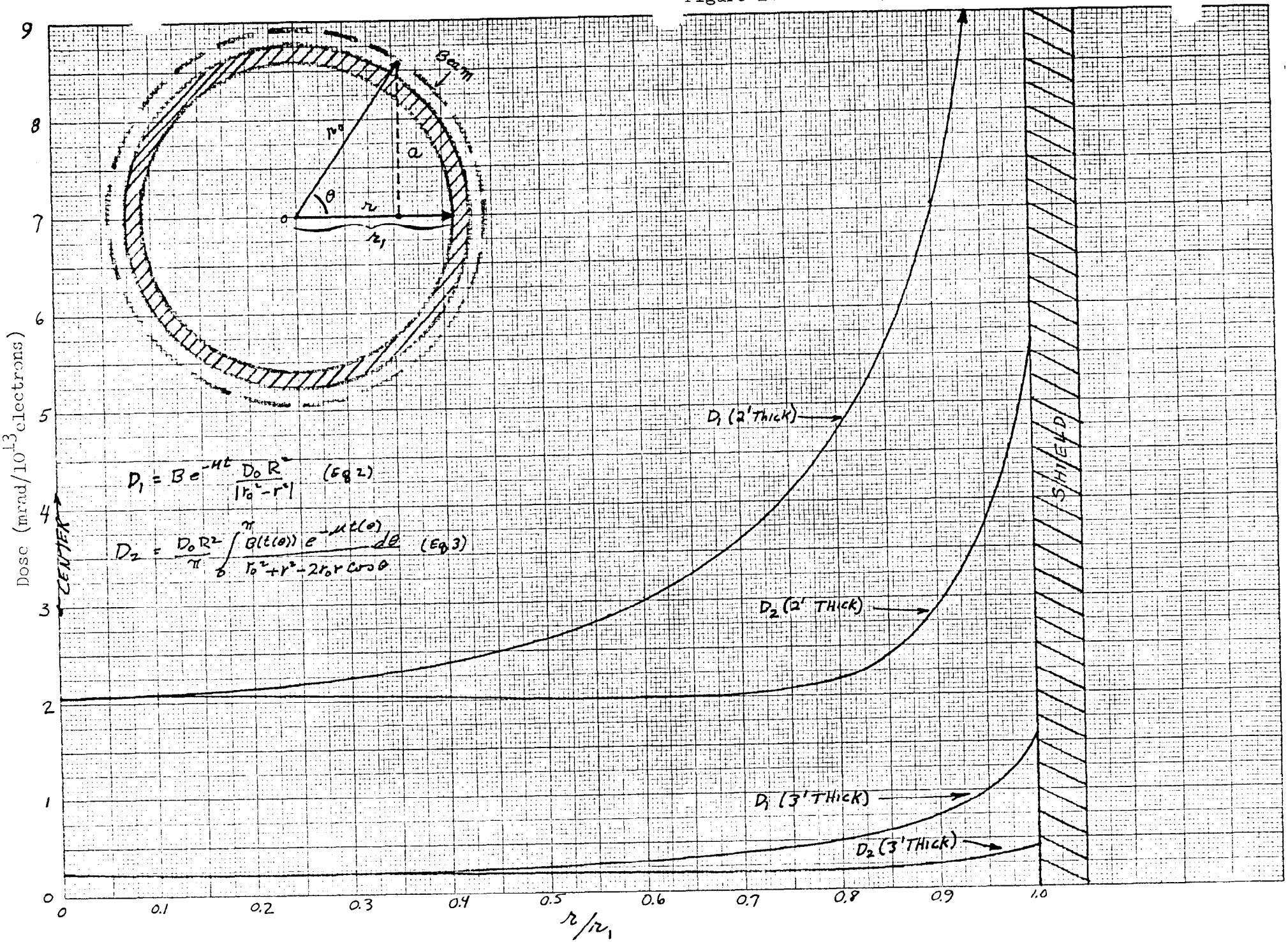
Beam
$r_0$
a
θ
r
$r_1$
o
$D_1$ (2' THICK)
$D_2$ (2' THICK)
$D_1$ (3' THICK)
$D_2$ (3' THICK)
SHIELD
CENTER
$D_1 = B e^{-\mu t} \frac{D_0 R^2}{|r_0^2 - r^2|}$ (Eq 2)
$D_2 = \frac{D_0 R^2}{\pi} \int_0^{\pi} \frac{G(t(\theta)) e^{-\mu t(\theta)}}{r_0^2 + r^2 - 2 r_0 r \cos\theta} d\theta$ (Eq 3)
Dose (mrad/$10^{13}$ electrons)
$r/r_1$
0
1
2
3
4
5
6
7
8
9
0.1
0.2
0.3
0.4
0.5
0.6
0.7
0.8
0.9
1.0